

MICROSTRUCTURE-PROPERTY RELATIONSHIPS AND THE NDE OF CONCRETE DAMAGE AND FRACTURE

ERIC N. LANDIS* AND JOHN E. BOLANDER†

*University of Maine
Department of Civil & Environmental Engineering
Orono, Maine 04469, USA
e-mail: landis@maine.edu, <http://www.civil.umaine.edu>

†University of California - Davis
Department of Civil & Environmental Engineering
Davis, California 95616, USA
e-mail: Jebolander@ucdavis.edu, <http://cee.engr.ucdavis.edu>

Key words: Nondestructive Evaluation, X-Ray Computed Tomography, Image Analysis, Lattice Models, Fracture

Abstract. The key to successful nondestructive evaluation (NDE) of complex heterogeneous materials is to focus not only on the interrogation technique, but how the measurement is related to the desired performance property. In this work, the focus is on key microstructural features that can be directly measured, and how we can use those measurements to predict performance of heterogeneous civil engineering materials. Not surprisingly, the key is to focus on microstructure, and to appropriately match the interrogation techniques with the models that can predict strength, toughness, durability, and other properties of interest. We find that numerical models developed to directly mimic micro-mechanical phenomena offer great promise for making a robust nondestructive measurement-performance link. As examples, particle-based and lattice-based models allow incorporation of measurable microstructural features such as porosity and pore size distribution, phase distribution, as well as other spatially varying properties such as moisture. Examples are presented where x-ray tomography is used to produce 3D images of concrete microstructure, and how that information is can be incorporated into spatially matched numerical models to predict performance. The argument is made that physically based models for micromechanical phenomena represent the next step towards a viable NDE system for complex civil engineering materials.

1 INTRODUCTION

Nondestructive evaluation (NDE) has long played an important role in the life cycle of different materials and structures. When properly applied, NDE can lead to an objective way to optimize service life and to allocate finite resources for restoration and repair. A model use of NDE can be seen in the aerospace industry, where NDE is integrated into the structural life cycle through “damage tolerant design.” In this

approach, regular inspection intervals are coupled with quantitative criteria for continued use, repair and retrofit, and ultimately, retirement.

The reason this approach is so successful in that industry is that for the primary materials being used (most notably aluminium alloys and other metals), a robust fundamental framework exists for relating relevant microstructural features to overall material performance. Linear elastic fracture mechanics, along with associ-

ated nonlinear fracture models, can be used to evaluate both ultimate structural capacity and fatigue life. As a result, appropriate nondestructive testing techniques, such as ultrasound, electromagnetics, and simple visual inspection, can be optimized for measuring crack sizes. Once an accurate crack size is measured, the appropriate fracture theory may be used to predict performance.

Unfortunately, concrete and concrete structures do not lend themselves to such a nicely defined inspection and evaluation protocol. Firstly, the heterogeneous structure of the material is by nature difficult to quantify. Porosity and pore size distribution, cracks, defects, aggregates, and interfaces all defy a simple characterization. Secondly, even if one could completely characterize the material structure, we do not have a robust framework from which we can make quantitative performance predictions.

The purpose of the work described in this paper is to consider both the interrogation and evaluation sides of the NDE problem as they apply to concrete structures. However, the focus is on ways we might be able to predict performance given a reasonable representation of microstructure. The thesis presented (which will be neither accepted nor rejected) is that quantitative nondestructive evaluation of concrete structures must be based on microstructural features that are directly measurable. In this paper we present a potential path for NDE-microstructure-property link.

2 Nondestructive evaluation of concrete

Historically, the most common NDE techniques for concrete relied on purely empirical techniques that related the interrogation method with the property of interest, as best exemplified by the rebound hammer. The fundamental basis for the relationship between hammer response and compressive strength is, however, tenuous at best. The weak fundamental basis leads to narrow applicability as well as significant scatter in the predictions.

The last 25 years has seen an increase in quantitative NDE techniques for concrete, as

perhaps best exemplified by the impact-echo technique for locating cracks, voids, or delaminations. While the technique is fairly well established, and is effective at locating defects, our ability to turn that measurement into a robust performance prediction is limited.

There is not an easy solution to the NDE problem for concrete. Material complexity, moisture effects, and age effects all influence the microstructure-property relationships that would allow us to predict performance. In this work, we use information obtained from a high resolution imaging technique to quantitatively examine some microstructure-property relationships and examine how we might be able to exploit them for performance prediction.

3 Experimental measurements

3.1 X-ray microtomography

The microstructural imaging technique used in this work is referred to as X-ray Microtomography (XMT). XMT produces a 3-dimensional map of an object's x-ray absorption through the mathematical reconstruction of a series of 2-dimensional radiographic images taken over many different rotation angles. The technique is perhaps best known for its use in medical imaging, where it is referred to as a CAT-scan. Different material phases typically exhibit characteristic x-ray absorption, and, as such, the 3-dimensional map may be interpreted as a material phase map. XMT has gained relatively wide usage for a wide range of materials applications [1] and its use is growing thanks to the increasing availability of both laboratory-scale instruments and synchrotron-based facilities. In the work described here, we used a synchrotron x-ray source that allowed us to make very high contrast images. The geometry of the synchrotron source limited our specimens to very small (nominally 5 mm diameter by 4 mm high) cylinders of portland cement mortar. The small specimens allowed us to have a relatively high spatial resolution of 6 micrometer pixels.

3.2 Specimens

The specimens used here were prepared using a high early strength (ASTM Type III) portland cement, very fine silica sand (pass #80 sieve), small glass bead aggregates, and water. The glass beads were used for their well-defined geometry and because the bead surfaces can be easily modified to change interface properties. In this work, two different surfaces were considered: smooth (untreated) and etched using an ammonium bifluoride solution. The mix proportion was 1 : 0.64 : 0.23 : 0.45, by weight cement : fine sand : glass beads : water. Additionally, a set of specimens without glass beads was prepared to investigate properties of the cement matrix. The material was mixed with a bench top rotary mixer and cured in wet conditions for seven days. The small cylindrical test specimens were extracted from the bulk material using a 5.5 mm inside diameter diamond coring bit. Resulting cores were then cut to a nominal 4 mm length.

3.3 Experiments

An experimental protocol was established such that changes in internal structure could be tracked from undamaged to damaged states. A custom load frame was constructed that allowed us to make 3D tomographic images of specimens under load while simultaneously monitoring load and deformation information. The first tomographic scan is made of the specimen mounted in the load frame prior to any load being applied. Once the first scan is complete, a load is applied and the second scan is made with the specimen under load. The nominal plan for each specimen was to make a scan at: 0% and 90% of peak load, as well as a post-fracture scan. Since the exact strength of each individual specimen was not known a priori, these percentages were approximate.

Fig. 1 illustrates the results of a tomographic scan, where the data can be displayed either as a 2D slice or a 3D rendering (Fig. 1(b)). A typical scan sequence is illustrated in Fig. 2, where a series of slice images oriented parallel to the axis of load are shown, highlighting the

splitting nature of failure. Fig. 2(a) shows an undamaged specimen. The flat regions above and below the specimen are the steel loading platens. In the image of Fig. 2(b), which was taken at roughly 97% of peak load, a fine crack has formed through the center of the specimen. It should be noted that this crack does not extend through the entire length of the specimen. In the image of Fig. 2(c), taken post peak load, the crack has opened, and has branched near the top and bottom platens. It can be seen in Fig. 2(b) and 2(c) how the aggregate particles can deflect and redirect the cracks.

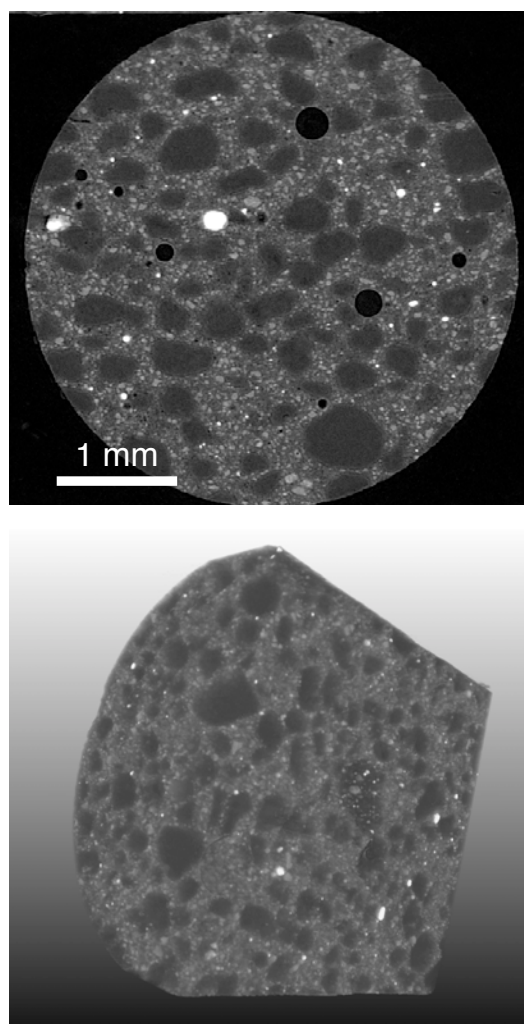


Figure 1: Illustration of microtomographic slice image (above) and 3D rendering (below). Variations in x-ray absorption within the material allows one to observe different microstructural phases.

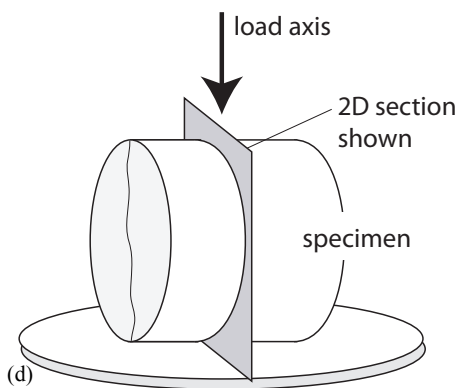
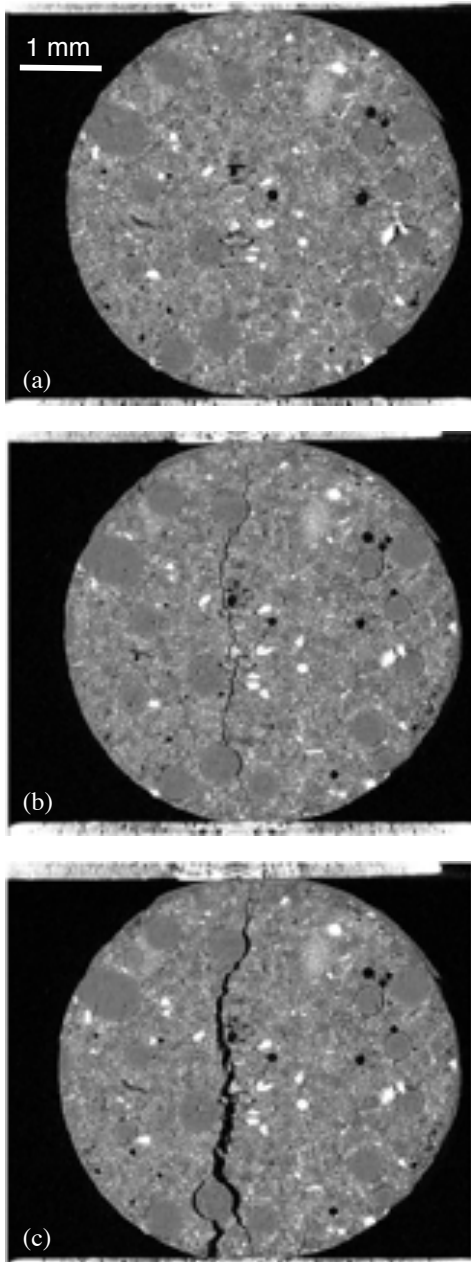


Figure 2: Image sequence illustrating progression of split cylinder fracture.

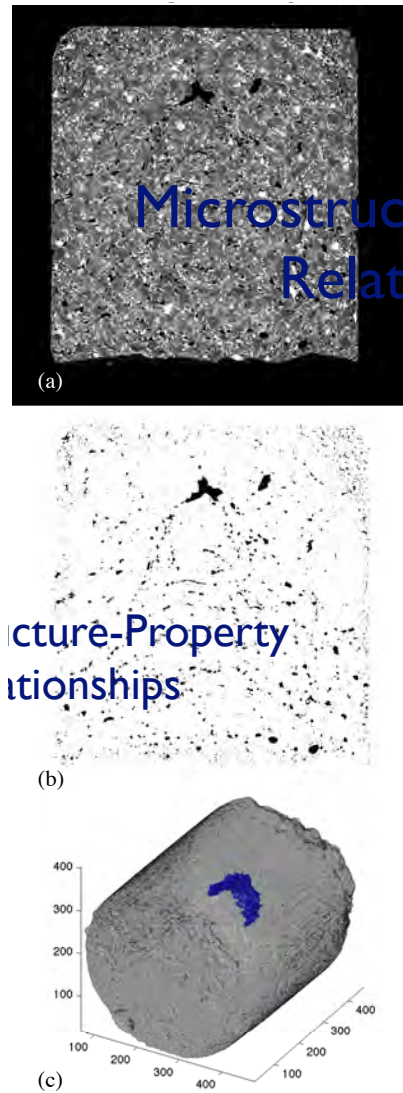


Figure 3: Illustration of grayscale slice (a), corresponding pore system (b), and 3D rendering of specimen with largest pore object highlighted (c).

3.4 3D Image Processing

The digital nature of the 3D images created by XMT allow us to make numerous quantitative microstructural measurements. In this work, we are focused on two things: porosity and pore size distribution, with particular interest in the largest flaw size. These measurements are made as follows. First, a threshold is applied to the grayscale images to produce a binary image. The threshold value is chosen as the voxel intensity that best represents the cutoff between solid and void. The process is illustrated in Fig. 3, where a grayscale slice (Fig. 3(a)) is segmented into a binary image (Fig. 3(b)), where

void space is shown as black, and solid material is shown as white.

Once an image is segmented, we can perform an analysis of the resulting void objects using a fast 3D connected components algorithm [2], that leads to the identification and measurement of each black (void) object in the image. From this analysis, porosity is simply the fraction of void objects in the specimen, and pore size distribution is determined by sorting the measured void object volumes. The largest void object, which is frequently of interest in failure analysis, can easily be identified from the connected components analysis. An example 3D rendering of a specimen with its largest void object highlighted is shown in Fig. 3(c).

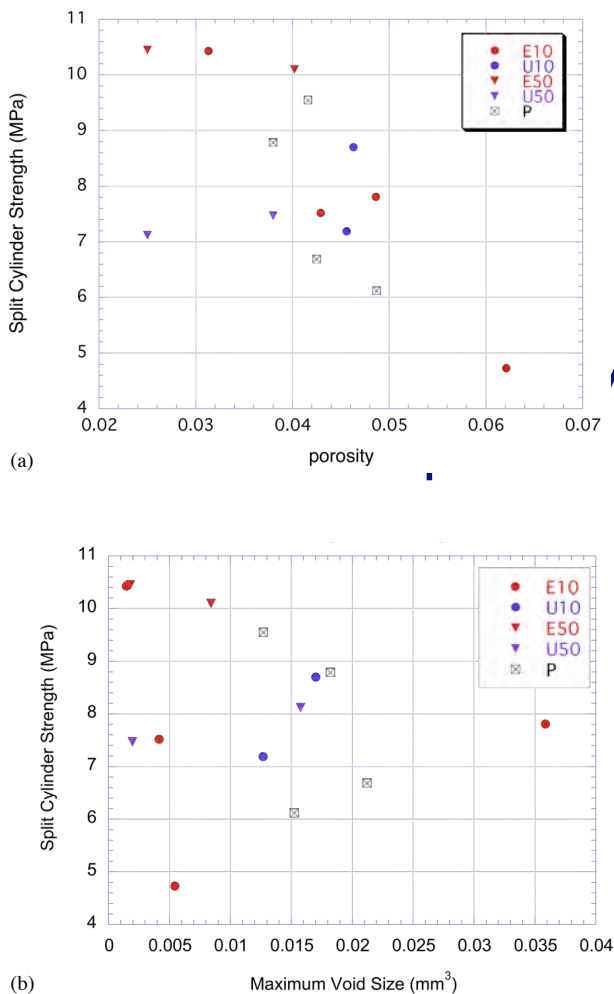


Figure 4: Plots of split cylinder strength versus porosity (a) and maximum void size (b).

3.5 Porosity and Pore Size - Strength Relationships

The pore structure measurements described in the previous section can then be used to examine how they relate to bulk material properties, such as split cylinder strength. Fig. 4(a) shows a plot of split cylinder strength as a function of overall specimen porosity. The data plotted includes five specimen types: E and U, for etched and unetched aggregates respectively. For the etched and unetched aggregates, weight fractions of 10% and 50% were considered separately. Thus “E10” refers to a specimen with 10% etched aggregates. Plain cement paste specimens are denoted by P.

As one might expect, there is a clear downward trend shown. Specimens with higher overall porosity tended to be weaker than specimens with lower porosity. There is sufficient scatter in the relationship to render any predictive relationship somewhat tenuous. Fig. 4(b) shows a similar relationship; however, in this figure the independent variable is the largest void object. Basic fracture theory dictates that the largest flaw should dictate the rupture strength, but this work shows that there is even more scatter than was found when we related split cylinder strength to bulk porosity. Fracture theory suggests, of course, that it is not flaw size alone that dictates fracture strength, but rather what flaw causes the greatest stress intensity or the greatest strain energy release. Thus, it is not simply an issue of flaw size, but flaw shape and flaw location.

We focused here on porosity and pore sizes partly because of their relevance in fracture strength, but also because they represent physical properties that can potentially be measured in the field. The level of scatter shown in Fig. 4 indicates that perhaps a direct measurement of porosity and/or pore size distribution may not be enough for a robust performance prediction. Before giving up completely on the matter, we explore more complete representations of the material. Specifically, as detailed below, we employed computational models that have a direct correspondence with the physical

microstructure of the specimen.

4 Modeling

4.1 Lattice Formulation

Lattice representations of heterogeneous materials have been used for a number of years, emerging from work in statistical physics [3]. The philosophy of the approach used here is that statistical variations and disorder can be explicitly represented in a way that resembles the actual material.

In the approach applied here, lattice topology is based on the Delaunay tessellation of nodal points within the specimen domain. The dual Voronoi tessellation defines the elastic and fracture properties of the lattice elements [4]. This discretization involves a three-phase representation of the material meso-structure as follows: hardened cement paste, aggregates, and cement-aggregate interface.

4.2 Matched Real and Virtual Specimens

In addition to the qualitative assessments that can be made from the images, we can also employ 3D digital image analysis methods to extract quantitative measurements. Relevant to the work reported here are efforts to create a matched set of real and virtual specimens for subsequent study. To do this, the spherical aggregates in the tomographic scans were isolated and their coordinates determined using a variance filter. Traditional intensity-based segmentation does not work because the voxel intensities of the glass aggregates are in the same range as the cement hydrates. However, because of the relative homogeneity of the glass beads, one can simply determine the variance of all voxels in a region. In regions where the variance is high we can assume the region is made up of cement hydrates and fines. Where the variance is low, we can assume the region is aggregates or voids. To distinguish bead aggregates from voids, we simply return to the original grayscale image, where voids were already identified by their low intensity.

Once the aggregates are located in the real specimen, the coordinates of the centroids rela-

tive to an overall specimen reference frame can be calculated and used to create a companion virtual specimen, as shown in Fig. 5. Here a virtual mesh is generated based on the measured aggregate centroids and diameters. Mesh properties can then include separate aggregate and paste phases, as well as an interface phase.

Matching the real and virtual specimens allows us to examine things that are otherwise difficult to measure. For example, the nature of the tomographic scans only allows us to examine the specimen at discrete points in time while the load is held static. In the virtual specimens we can also examine dynamic phenomenon and subtle increments in crack growth.

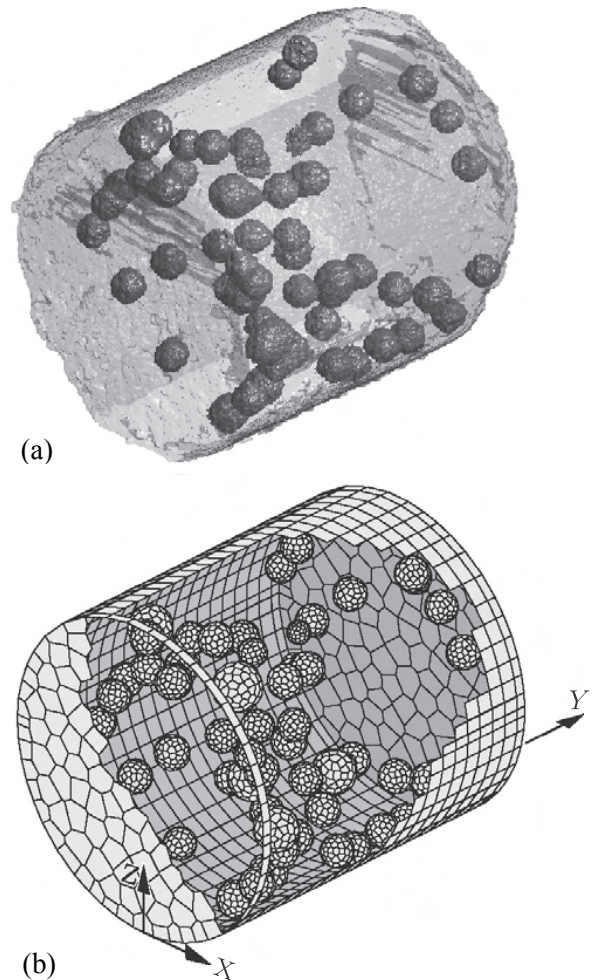


Figure 5: 3D renderings of bead aggregates in both real (a) and virtual (b) specimens.

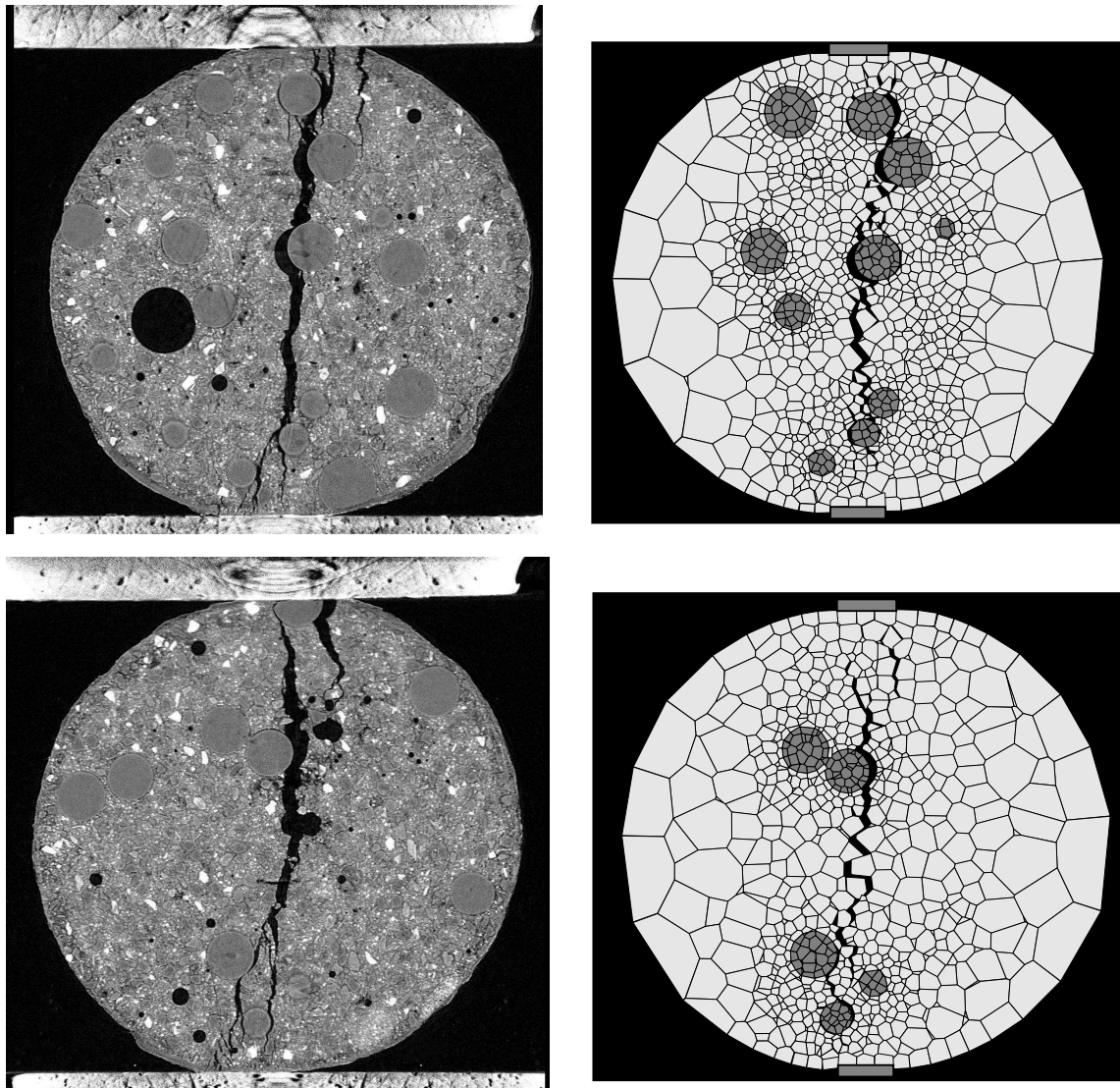


Figure 6: Comparison of damage in real and virtual specimens.

4.3 Virtual Experiments

Using volumes generated from matched real specimens, simulations on virtual split cylinder specimens were run. Details of the mesh properties are presented in [5]. Images illustrating the simulations are shown in Fig. 6, where virtual specimens are compared qualitatively with real specimens. The real specimens shown had unetched aggregates and a volume fraction of about 10%. The images highlight the ability of the discrete element model to capture physical fracture phenomena. Specifically, the role of the aggregates in redirecting cracks and branching cracks can be clearly observed. It should be

noted that to save meshing time, aggregates on the extreme outer edges are not meshed. Clearly the fineness of the mesh in the paste phase affects the tortuosity of the cracking, but with continued improvements in computational efficiencies, we will likely see numerical solutions that converge on the patterns of the real specimen.

5 DISCUSSION AND CONCLUSIONS

The results of the matched model simulations are encouraging and discouraging at the same time. They are encouraging because we are able to capture actual damage patterns and the corresponding load-deformation response

of the real specimens. The implication is that given sufficient computational power and microstructural information, we should be in an excellent position to make robust predictions. The discouraging aspect is that the results highlight the difficulty with NDE of concrete. Specifically, it was found that there is significant scatter in simulated strength even when the only varying parameter is the location of the aggregates [5]. Since no practical field measurement technique can give us this degree of resolution, accurate prediction remains an elusive goal.

Despite the discouraging aspects for field application, we stand by the notion that we must continue to develop technologies and techniques for relating field-measurable properties to bulk material performance parameters. Such technologies will be critical in overall condition assessment as well as rational decisions in allocation of resources.

6 ACKNOWLEDGMENTS

The authors gratefully acknowledge the support of a collaborative grant from the U.S. National Science Foundation (0625030 and 0625593). The authors further acknowledge the contributions of students D. Asahina (UC-

Davis), S. de Wolski (UMaine), and L. Flanders (UMaine).

REFERENCES

- [1] Stock, S.R. 2008. Recent advances in x-ray microtomography applied to materials *International Materials Reviews* **53**:129–181.
- [2] Franklin, W. R. 2009. CONNECT - find 3D connected components. <http://wrfranklin.org/pmwiki/Connected-Components>.
- [3] Herrmann, H.J. and Roux, S. (eds.) 1990. *Statistical Models for the Fracture of Disordered Media*. North-Holland.
- [4] Berton, S. and Bolander, J.E. 2006. Crack band modeling of fracture in irregular lattices *Computational Methods in Applied Mechanics and Engineering* **195**:7172–7181.
- [5] Asahina, D., Landis, E.N. and Bolander, J.E. 2011. Modeling of phase interfaces during pre-critical crack growth in concrete *Cement and Concrete Composites* **33**:966–977.